International Journal of Solids and Structures 46 (2009) 2650–2658

Contents lists available at ScienceDirect

International Journal of Solids and Structures

journal homepage: www.elsevier.com/locate/ijsolstr

The influence of particle shape, volume fraction and distribution on post-necking deformation and fracture in uniaxial tension of AA5754 sheet materials

Xiaohua Hu [a,*], David S. Wilkinson [a], Mukesh Jain [b], Raja K. Mishra [c]

[a] Department of Materials Science and Engineering, McMaster University, 1280 Main Street West, Hamilton, Ont., Canada L8S 1J4
[b] Department of Mechanical Engineering, McMaster University, Hamilton, Ont., Canada L8S 1J4
[c] General Motors Research and Development Center, Mail Code 480-106-212, 30500 Mound Road, Warren, MI 48090-9055, USA

ARTICLE INFO

Article history:
Received 5 December 2008
Received in revised form 30 January 2009
Available online 27 February 2009

Keywords:
Aluminum alloy
Strain localization
Fracture
Particles
Distribution

ABSTRACT

Finite element analysis was performed over a small particle field, edge constraint plane strain post-necking model. The aim is to understand the roles of particle shape, volume fraction and distribution over the post-necking deformation and fracture of AA5754-O sheet materials. For models containing one single particle, the post-necking deformation decreases when the particle varies from circular to elliptical. The inter-particle spacing, the major parameter of distribution to determine whether a pair of particles belongs to a stringer or not, was varied for models with two particles of circular or elliptical shape. The general trend is that the post-necking deformation and fracture strains decrease with decreasing spacing between particles. There is considerable difference in terms of both fracture topographies and strains for models containing 16 particles when distributions varied from random/uniform to stringer distributions. The post-necking deformation and fracture strains monotonically decrease with particle volume fractions for models with 4–64 particles of random or stringer distribution. This indicates that the post-necking behavior for AA5754-O alloys where the matrix material is rather ductile is not solely controlled by a single or pair of particles although they may become initiation places of damage. Multiple damaging sources such as stringers or large particles can act cooperatively and speed up the damaging propagation of the material, and therefore produce small post-necking deformation and early fracture. The center clustering of particles can be beneficial for post-necking behavior and bendability of sheet materials.

1. Introduction

AA5754 aluminum sheet alloys are candidates for car inner panels and car body structures for light weight, fuel efficient cars. The major hurdle of using such alloys, however, is its high cost of production by the conventional direct chill (DC) cast technology. Therefore, prime interests of research have been put on the much cheaper alloys produced by continuous strip casting (CC) recently. The use of CC alloys to replace DC alloys, however, requires the CC alloys to have better or at least similar formability as many car body structures involve stamping or hemming processes. Extensive experimental uniaxial tension studies have shown that the CC and DC alloys are similar in formability in terms of localization strains, while the post-necking deformation of the CC alloys, which determines the final fracture strain, is much less (Kang et al., 2007). Inferior bendability is observed in CC alloys, too. From the model of Datsko and Yang (1960), the two properties, i.e. the fracture limit and bendability are connected. The bendability is important for auto door panel flanging and hemming processes (Carsley and Kim, 2007). The similarity and dissimilarity between the two alloys have been linked to the material microstructures. The localization strains of the alloys are postulated to be mostly controlled by the grain level inhomogeneities, while post-necking deformation is more linked to the particle distributions. The grain structures and texture of the tested CC and DC alloys are similar. DC alloys have more random particle distribution, while the particles in CC alloys are distributed as stringers aligned along the rolling direction.

This postulation seems to have been proven by our microstructure-based finite element studies which adopt a two-stage modeling procedure (Hu et al., 2008a). The plane stress pre-necking (from uniaxial tension to localized necking) model shows that the grain structures play a dominant role in this deformation regime (Hu et al., 2008a; Hu et al., 2007; Hu et al., 2008c). The edge constraint post-necking model, on the other hand, explains the experimental observation of different fracture topographies and fracture limits between the two alloys: CC alloys have more

* Corresponding author.
E-mail address: huxiao@mcmaster.ca (X. Hu).

0020-7683/$ - see front matter © 2009 Elsevier Ltd. All rights reserved.
doi:10.1016/j.ijsolstr.2009.02.012

propensity of shear type failure and considerable less fracture strain, while DC alloys show cup–cone type failure and large fracture strain. The post-necking model shown by Hu et al. (2008a), however, uses a particle field with a domain size of $92 \times 70\ \mu m^2$ cut from optical microstructure of AA5754 CC and DC alloys with identical Fe content of 0.21%. The volume fractions of particles are very much related with the Fe level in the alloys. The statistical distribution of the domains, in terms of particle shape, particle volume fracture and stringer volume fraction, may not be representative of the whole material. Systematic studies of the influences of these parameters are lacking. A parametric study has been performed by large particle field models which consist of thousands of particles where each particle is simplified as by a single square element. This current work will concentrate on a more refined representation of particle shapes as circular or elliptical. To represent such shapes in finite element models requires a lot of elements. Therefore it is non-tractable at present to generate and simulate models containing a large number of particles with well defined shapes and fine meshes. Therefore, this current work will use models of small particle fields containing 64 particles at most. In most of the models, the particle volume fractions are kept at 2%, therefore the model size will vary for 1, 2 and 16 particle models, except in the case when particle volume fraction are studied where the model sizes are kept constants for models of different number of particles.

It must be noted that the results of the small particle field models does not quantitatively reflect the experimental fracture strains of actual material, but can be used as a qualitative relative comparison of the influences of different parameters on post-necking deformation and fracture. The single particle models focus on the influences of particle shape and the two particle model on inter-particle spacing, while the 16 particle models emphasize the different particle distribution. Further, the positioning of particles, e.g. the particles are located at the center of models containing one or two particles and diagonal positioning of stringers, is chosen to have easy comparability between models.

2. Modeling

As described in Hu et al. (2008a), the edge constraint post-necking models study the deformation regime from the onset of localized necking to final fracture. The model is developed according to the theoretical analysis of deformation instabilities stages during uniaxial tension (Hu et al., 2008a). The original development assumes the model domain as that of a cross-section of the localized necking band and perpendicular to the direction of the band (BD), i.e. RD′ × ND (see the pink frame of dashed lines in the center of the localized necking band sketched in Fig. 1). Later modification (Hu et al., submitted for publication) is made to assume the modeled cross-section to be parallel to the RD × ND plane (see the red frame in the center of the localized necking band sketched in Fig. 1)[1] when the samples are loaded along the rolling direction. RD and ND stand for rolling and normal directions of sheet materials, respectively. Fig. 2 shows an example of the model containing 9 particles of uniform deformation.

Velocity boundary conditions are applied to the left (Le) and right (Re) edges along the RD (x_1) direction, while the deformation of the two edges are constrained along the ND (x_2) direction,

$$\begin{aligned} v_1|_{x_1=Le} &= -v \quad v_2|_{x_1=Le} = 0 \\ v_1|_{x_1=Re} &= v \quad v_2|_{x_1=Re} = 0 \end{aligned} \tag{1}$$

The top and bottom edges are free to deform in both degrees of freedom.

The dimension of the ND direction (x_2) of the model, e.g. the thickness of an uniaxial tension sample, is termed as t, while that of the width of the cross-section (RD-x_1) of the localized necking band is denoted as b. Similar to (Hu et al., submitted for publication), the ratio between t and b is fixed to 10/7.

The ABAQUS/EXPLICIT finite element package is utilized (ABAQUS Inc., 2006). An isotropic elasto-plastic rate-independent user material model is used to represent the constitutive behavior of the matrix aluminum material (Hu et al., 2008a). The input flow curve of the matrix material is assumed to follow a Holloman law based on a three-stage fitting of the tensile test results of an AA5754 DC alloy (Hu et al., 2008a).

$$\bar{\sigma} = k_i \bar{\varepsilon}^{n_i} \tag{2}$$

where the parameters of the DC alloy in these equations is shown in Table 1.

It must be noted that as the present model represents the post-necking deformation regime, the model assumes that localized necking will immediately start when the simulation begins. There-

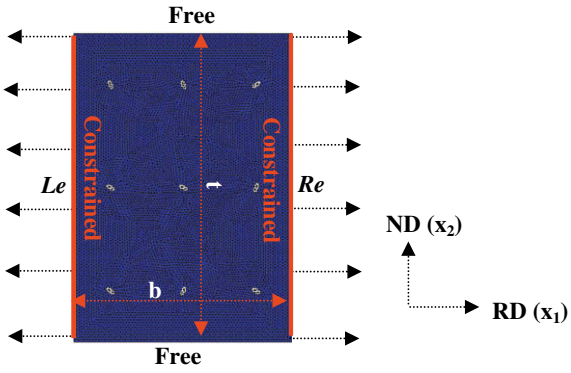

Fig. 2. An example of the edge-constraint plane strain post-necking model.

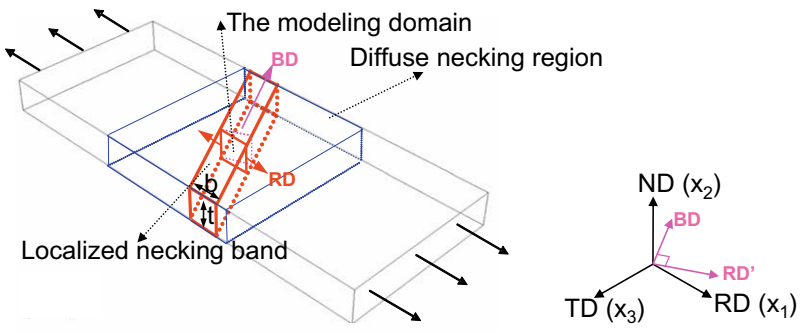

Fig. 1. A sketch showing the modeling domain of the edge constraint plane strain post-necking model.

Table 1
Holloman parameters.

i	Strain ranges	k_i	n_i
1	$\varepsilon \in (0,0.0235)$	421.8	0.2613
2	$\varepsilon \in (0.0235,0.0926)$	570.1	0.3413
3	$\varepsilon \in (0.0926,-)$	396.6	0.1891

fore an initial equivalent strain ε_0^p, i.e. the localized necking strain, is assigned to the matrix material. The strain can be deduced from the maximum tension condition (Marciniak et al., 2002) for stretching of a continuous sheet of an isotropic material,

$$\frac{d\sigma_{11}}{d\varepsilon_{11}} = (1+\beta)\sigma_{11}, \text{ where } \beta = \frac{\varepsilon_{22}}{\varepsilon_{11}} \tag{3}$$

where β is -0.5 for uniaxial tension. The value is determined to be around 0.36 according to Eqs. (2) and (3), and parameters listed in Table 1.

From careful experimental observations of long cross-section (RD × ND) of the fractured sample, very few voids were found in the regions near the fractured surface of the AA5754 alloys. It has been concluded that the matrix material is rather ductile and the major mechanism leading to matrix material failure is the excessive shear localization (Sarkar et al., 2001; Sarkar et al., 2004). Therefore, a simple shear-type failure model is utilized where element deletion begins when the equivalent strain reaches a critical value,

$$\bar{\varepsilon}^p = \bar{\varepsilon}_c^p. \tag{4}$$

This critical equivalent strain $\bar{\varepsilon}_c^p$ can be also called the local fracture strain and a rather high value of 1.5 is chosen in the current study because of the high ductility of the matrix material. However, a more precise value is necessary and need to determined, e.g. experimentally, in the future in terms of quantitative predictions.

For the particles, linear elasticity is assumed to be the equivalent stress of $\sigma_p^0 = 0.8$ GPa as described before (Hu et al., 2008a), where the Young's modulus (E) is 210 GPa and Poisson's ratio (ν) is 0.28, respectively. An exponential non-linear equivalent stress–strain behavior is assumed afterwards (Hu et al., 2008a),

$$\bar{\sigma}_p = \sigma_p^0 + \left(\sigma_p^1 - \sigma_p^0\right)\left[1 - \exp\left(-g\bar{\varepsilon}^{nl}\right)\right] \tag{5}$$

where E is the elastic modulus, $\bar{\varepsilon}^{nl}$ is the non-linear equivalent strain and σ_p^1 is the saturation stress (here chosen to be 5 GPa) and

$$g = E/(\sigma_p^1 - \sigma_p^0) \tag{6}$$

This treatment will ensure the work hardening rate is equal to E at $\bar{\varepsilon}^{nl} = 0$ (Hu et al., 2006). The constitutive behavior of particles is represented by tabular data lines in the ABAQUS input file pre-calculated from Eq. (5). It should be noted that the properties of the second phase particles in AA5754 alloys are not available from the literature. The parameters, therefore, are chosen to be as that of cementite (Fe_3C) as reported by Hu et al. (2006) with the consideration that the particles are much harder than the matrix materials. With this condition, the choice of different parameters of particle properties will not drastically influence the results of model predictions.

Particle fractures have been observed at or near the fracture surface of the sample. Particles are $(Fe,M)_6Al$ or Mg_2Si intermetallics and they are brittle. Therefore both simple shear-type and tension-type failure models are applied. The shear-type failure model is that any of the elements in a particle will be deleted when the non-linear equivalent strain of this element reaches a critical value,

$$\bar{\varepsilon}^{nl} = \bar{\varepsilon}_c^{nl} \tag{7}$$

Here $\bar{\varepsilon}_c^{nl}$ is chosen to be 0.007, which corresponds equivalent stress of 2 GPa.

The tension-type failure is that the tensile hydrostatic stress σ_m reach a critical value,

$$\sigma_m = \sigma_m^c \tag{8}$$

The critical value is chosen to be 1.05 GPa.

It must be noted that all the parameters are arbitrarily chosen due to lack of experimental data from the literature, but the values are chosen with the consideration that the second phase particles are brittle compared with the matrix materials.

After the simulation, a macroscopic fracture strain measure is calculated according to the following equation (Hu et al., 2008a):

$$\bar{\varepsilon}^f = \varepsilon_0^p + 1.155\ln\left(\frac{t_0}{t_f}\right) \tag{9}$$

where t_0 is the initial thickness of the model before deformation and t_f is the minimum thickness measured after final fracture. The co-efficient of 1.155 is to transform from the strains of the plane strain deformation into equivalent strains. It is obvious that the variation of $\bar{\varepsilon}^f$ reflects the post-necking deformation as ε_0^p is constant.

3. Single-particle model

The single-particle model consists of a single particle of circular or elliptic shape embedded in the aluminum matrix. The dimension of the model is $t \times w = 7.5 \times 5.3\ \mu m^2$. The particle volume fraction in the model is 0.02, where the equivalent diameter of the particle is 1 μm. The two parameters will be kept the same for all the following simulations with 2 and 16 particles. The equivalent diameter $\bar{d}$ of a particle is that of a circular disk which has the same volume of an elliptic disk.

$$\bar{d} = 2(a \cdot b)^{0.5} \tag{10}$$

where a and b are the long and short axes of an ellipse, respectively.

The parameter studied is the shape factor ($r = a/b$, where a is the long axis and b is the short axis of an ellipse) of the particle where the long axis of the ellipse is parallel to the loading direction.

Similar to that in Hu et al. (2008c), the finite element analysis uses six-node triangular quadratic plane strain elements (CPE6M). Mesh strategies are used to make the finite element meshes to be approximately homogeneous, which is essential for comparability between models (Hu et al., 2007). The size of the triangular meshes (the edge of a triangle) is around 0.15.

Fig. 3(a)–(f) shows the fracture patterns for different shape factors. The contours shown are equivalent strains and the contour levels are not given since only the fracture patterns are of interest here.

The variations of the fracture strains calculated from Eq. (9) are shown in Fig. 4, which shows that the fracture strains decrease with increasing shape factor of ellipses.

4. Two-particle model

This model consists of a pair of particles of circular or elliptic shape ($r = 3$) embedded in the aluminum matrix. The dimension of the model is $10.6 \times 7.5\ \mu m^2$. The objective is to find the influence of relative equivalent inter-particle spacing and shape factor on fracture strains. The relative equivalent inter-particle spacing is expressed as,

$$\overline{R} = \frac{s}{\bar{d}} - 1 \tag{11}$$

where s is the distance between the centers of the two particles. As expression (11) uses equivalent diameter of grain $\bar{d}$, $\overline{R}$ is then a measure independent of particle shape factor.

The relative equivalent inter-particle spacing $\overline{R}$ varies from 0.2 to 2 for models containing circular particles and 0.6 to 2 for models

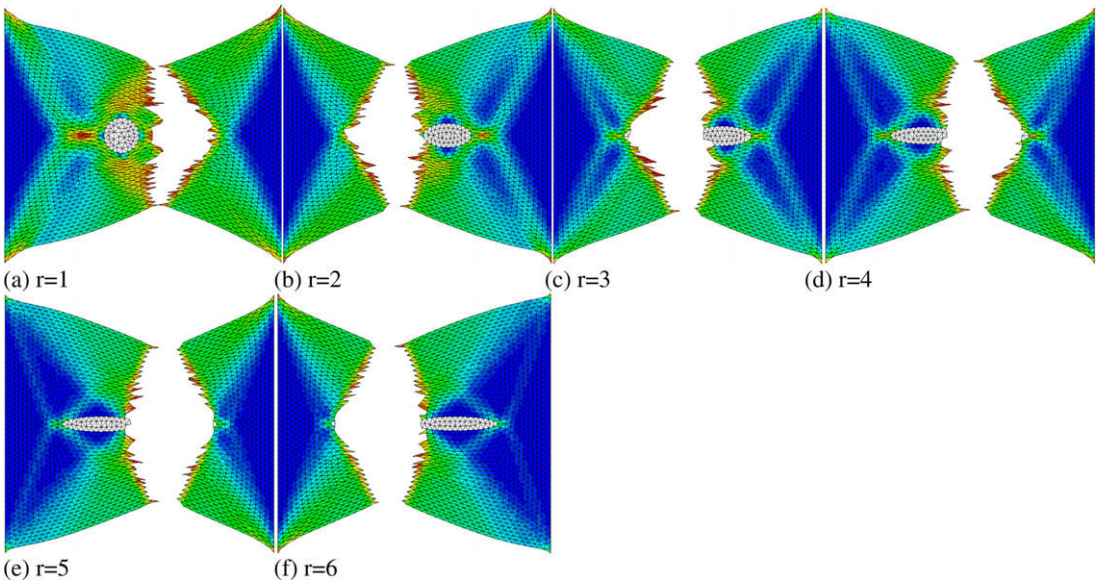

Fig. 3. The equivalent strain distributions and fracture patterns of the models after total fracture as a function of the shape factor *r*.

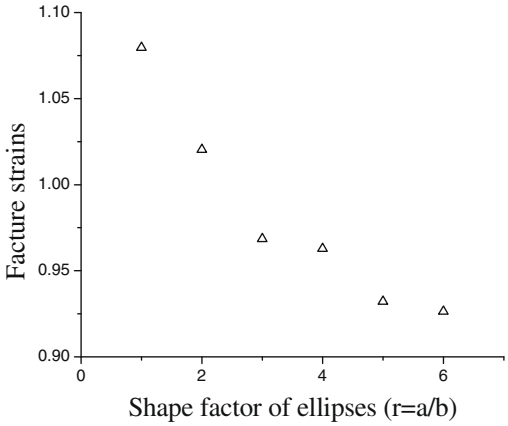

Fig. 4. The variations of fractures strains of the models with shape factor.

containing elliptic particles with the shape factor kept constant at $r = 3$. The two particles are in direct contact for the elliptical particles when $\overline{R} = 0.73$, therefore the result of $\overline{R} = 0.6$ is actually for a model containing one particle which is formed by two intersecting particles where the redundant part is removed.

Figs. 5(a)–(f) and 6(a)–(d) show fracture patterns for varying equivalent relative inter-particle spacing for models containing circular and elliptical particles, respectively. Fig. 7 shows the calculated fracture strains.

It is seen that the models containing elliptical particles show lower fracture strains than those with circular particles for identical relative inter-particle spacings. Fracture strains initially get smaller as the interparticle spacing increases then they rise sharply. This observation is different from our previous plane stress two-particle models where the localized necking strains monotonically increase with inter-particle spacing (Hu et al., 2007). For the plane strain model, the localization bands start from the two diagonals of the model and diffuse towards the vertical center line of the model. Fracture occurs along that line unless they interact with other localization or damage phenomena. When the two round particles are close together, e.g. $\overline{R} = 0.2$, the diagonal diffusing bands are hindered by the particles and become redistributed in a complex, wider band pattern due to the particle shielding effect (Chawla et al., 2002). This leads to less excessive deformation of the matrix material between the particles until it is assisted by particle damage (see Fig. 8(a)). When the separation is larger, e.g. $\overline{R} = 0.6$, the diagonal bands are not hindered, but assisted by the interaction between the particles. Thus damage starts in the matrix material (see Fig. 8(b)). This is not the case for the elliptical particles with a large shape factor, since the vertical dimension, e.g. the short axis, of the particle is small (see Fig. 8(c)). It must be noted that here the word 'damage' means 'crack initiation'.

5. Multi-particle model

5.1. Influence of particle distribution

The simulation results for the single- and two-particle models show that damage initiation is related to particles: particle breakage and large local strain in the matrix near the particles. As the particle or particle pair lies in the middle of the model, the damage propagation path is always along a line which is perpendicular to the load direction. This leads to a cup–cup configuration of the fracture surface due to the boundary constraints.

Now we consider models containing multiple particles and discuss the influence of particle distribution on post-necking behavior. First, we consider models containing 16 particles. Each particle is elliptical with an equivalent diameter of 1 μm and shape factor of 3. The size of the model is set as $42 \times 30\ \mu m^2$ to ensure the volume fraction of the particles remains at 2%. Different distributions of particles are examined.

(1)Particles clustered in stringers which are distributed along diagonals. Each stringer consists of 2–16 particles, respectively (see Fig. 9(a)–(e)).
(2)Particles distributed uniformly (Fig. 9(f)).
(3)Particles distributed randomly (Fig. 9(g)).

Fig. 10(a)–(g) shows the equivalent strain distributions after total fracture for these particle distributions. Fig. 11 shows the fracture strain evolution with the number of particles in the stringer as well as for random and uniform particle distributions. These figures show that particles clustered in stringers lead to considerably

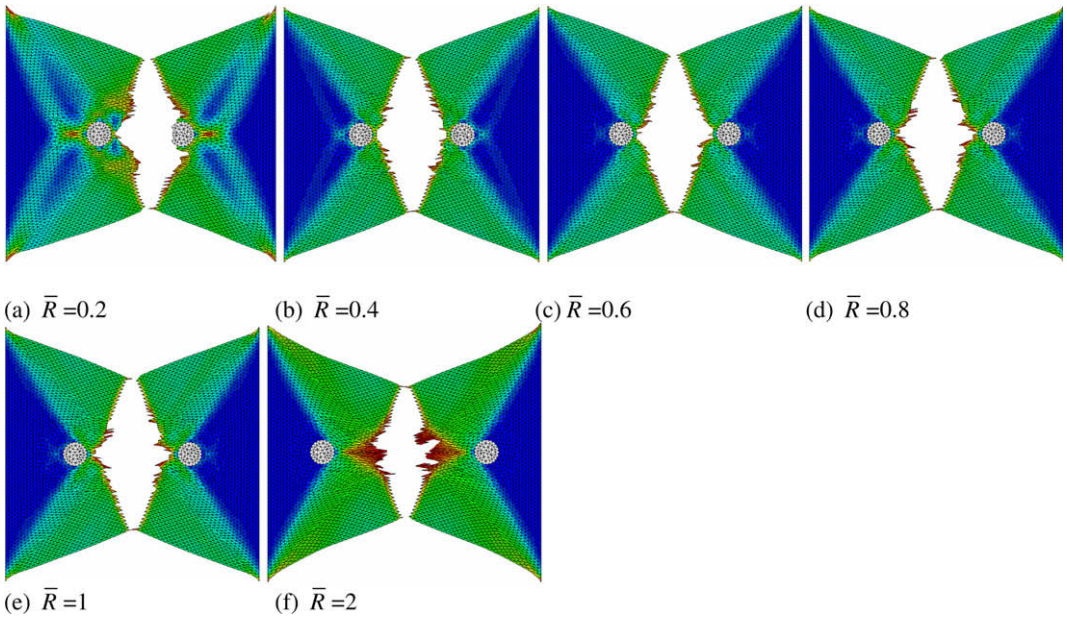

Fig. 5. The equivalent strain distributions and fracture patterns of the models after total fracture as a function of the relative equivalent inter-particle spacing in models containing circular particles.

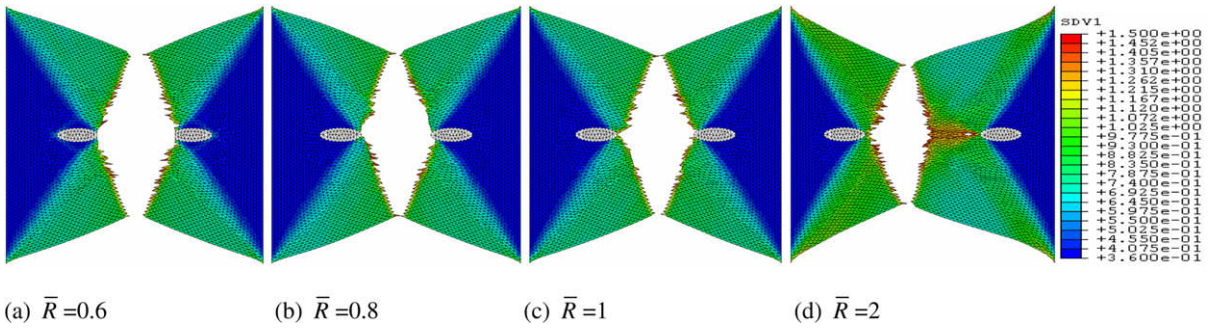

Fig. 6. The equivalent strain distributions and fracture patterns of the models after total fracture vary with the relative equivalent inter-particle spacing in models containing elliptic particles.

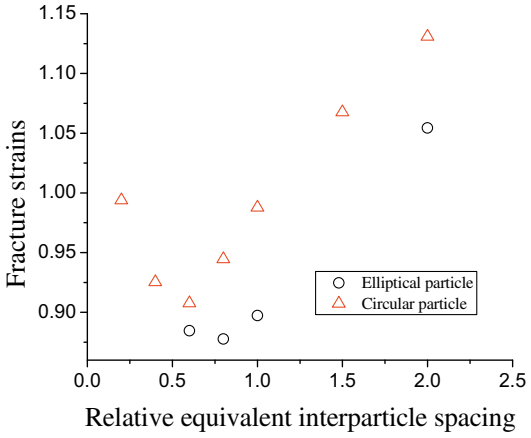

Fig. 7. The variations of fractures strains of the models with relative inter-particle spacing.

lower fracture strains than random or homogeneously distributed particles. The later models show identical fracture strains. For those models with particles clustered in stringers, stringers with 2 and 4 particles each lead to lower fracture strains than the model containing stringers with 8 particles (see Fig. 10(a)–(c)). These models show shear type failure. The model containing one single stringer in the middle of the model (see Fig. 10(d)) shows a cup–cup fracture feature similar to that of single- and two-particle models. This model has a fracture strain considerably higher than the multi-stringer models (Fig. 10(a)–(d)). The trend for models with stringers may be related to the number of active damage sources. The exception is that although there are 8 stringers shown in Fig. 10(a), the fracture strain is slightly higher than that for the model with 4 stringers (Fig. 10(b)). This suggests that stringers with 2 particles each are too short to pin the localization path, which can easily move away from the particles (see Fig. 10(g)).

5.2. Influence of particle volume fraction

We now consider the influence of particle volume fraction on post-necking deformation. Here we choose particle distribution configurations with stringers (4-particles in each stringer) aligned along the diagonal of the model (Figs. 9(b) and 12(a)–(d)). Homogeneously distributed particle models will also be discussed (Figs. 9(f) and 12(e)–(i)). The dimensions of the model, sizes and shape factors of particles are all kept the same as in the previously

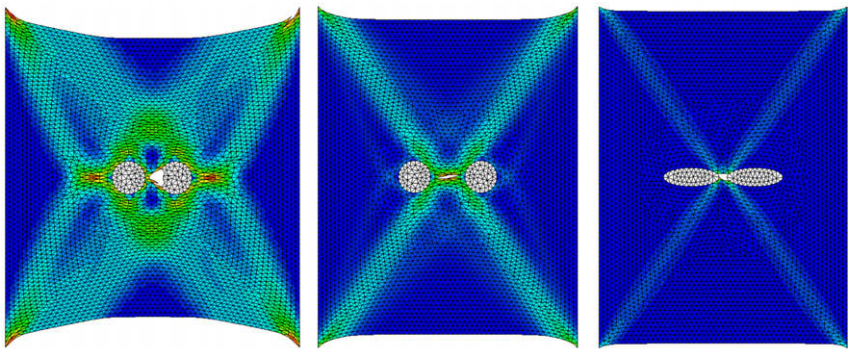

Fig. 8. The equivalent strain distribution for two particle models at the point when damage occurs. (a)–(b) For circular particle models when $\overline{R} = 0.2$ and 0.6, respectively. (c) For elliptic particle models when $\overline{R} = 0.8$ where the particles almost in direct contact.

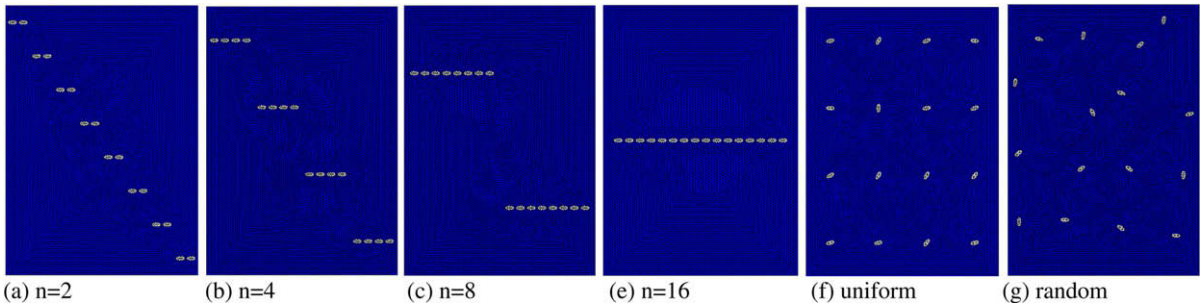

Fig. 9. Models containing 16 particles that are distributed differently.

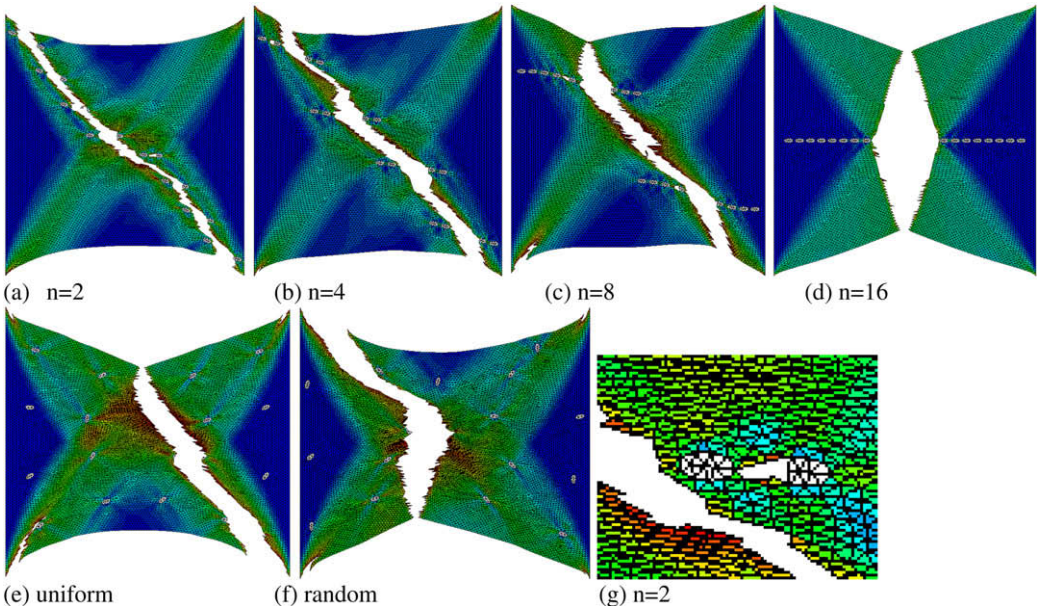

Fig. 10. The equivalent strain distributions and fracture patterns after total fracture in the models containing 16 particles.

discussed 16 particle model. The number of particles varies from 4 to 64, with volume fractions ranging from 0.5% to 8%.

The simulations using models shown in Fig. 12 combined with the results of Fig. 9(b) and (f) lead to the fracture strain variations with particle volume fraction shown in Fig. 13. All of the models with stringers containing 4 particles show shear type failure similar to that shown in Fig. 10(b), except when there is only one stringer which shows cup–cup fracture.

The models of the uniformly distributed particles do not show shear-type failure and show features similar to that shown in Fig 10(e) or (f). The fracture strains of the models with uniform particle distributions do not change drastically with volume fraction ranging from 0.5% to 3%. There is a drop in the fracture strain for higher volume fractions. The fracture strains for the models containing stringers are considerably lower and decrease rapidly with increasing volume fraction of particles up to about 2.0%.

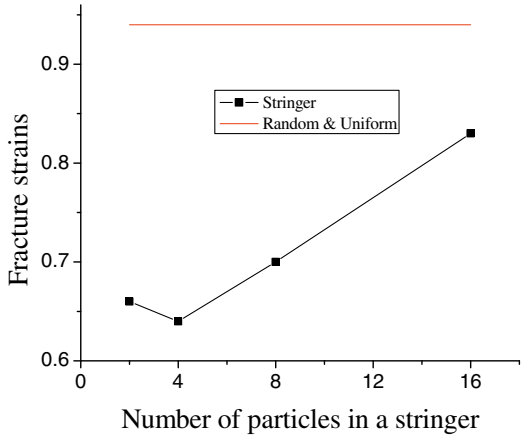

Fig. 11. Fracture strain evolution with number of particles in each stringer of particles in stringer distributions (the black lines with square symbols) in comparison with random and uniform distribution.

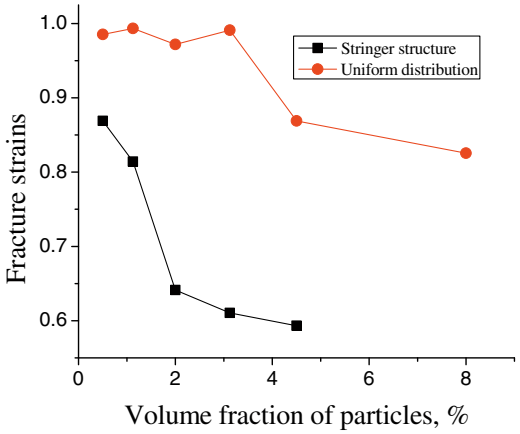

Fig. 13. The variations of fracture strains with volume fraction of particles for stringer structure models (the line with solid squares) and uniform distributions (the line with circles).

6. Discussion

For the single particle model, the post-necking deformation and fracture strains decrease when the particle varies from circular to elliptical. Models of one elliptical particle with higher aspect ratio of elliptical particle lead to lower fracture strains, due to high local strains induced in the region near the sharp edge of the particle. High stresses at the edge can lead to particle fracture.

The inter-particle spacing has been varied for models with two particles of circular or elliptical shape. The general trend is that the post-necking deformation decreases with decreasing spacing between particles. The exception is that there is slight increase of post-necking deformation with decreasing inter-particle spacing when the spacing is smaller than a critical value for the models consisting of circular particles due to the shielding effect. The models with elliptical shape show lower post-necking deformation and fraction strains than those with round particles. This is consistent with the results of single particle models, indicating that particles of large aspect ratio, e.g. long particles, are detrimental and can lead to early failure of the material. The results of the influence of inter-particle spacing show that stringers of small inter-particle spacing are more damaging due to large local strain induced between particles.

From the current studies, increasing particle volume fractions decrease the post-necking deformation and fracture strains. This is consistent with experimental tensile tests and bending tests of AA5754 alloys with different Fe content where alloys of higher Fe content consist of a larger volume fraction of particles (Sarkar et al., 2001). The influence of particle volume fraction indicates that the post-necking behavior for AA5754 alloys, where the ma-

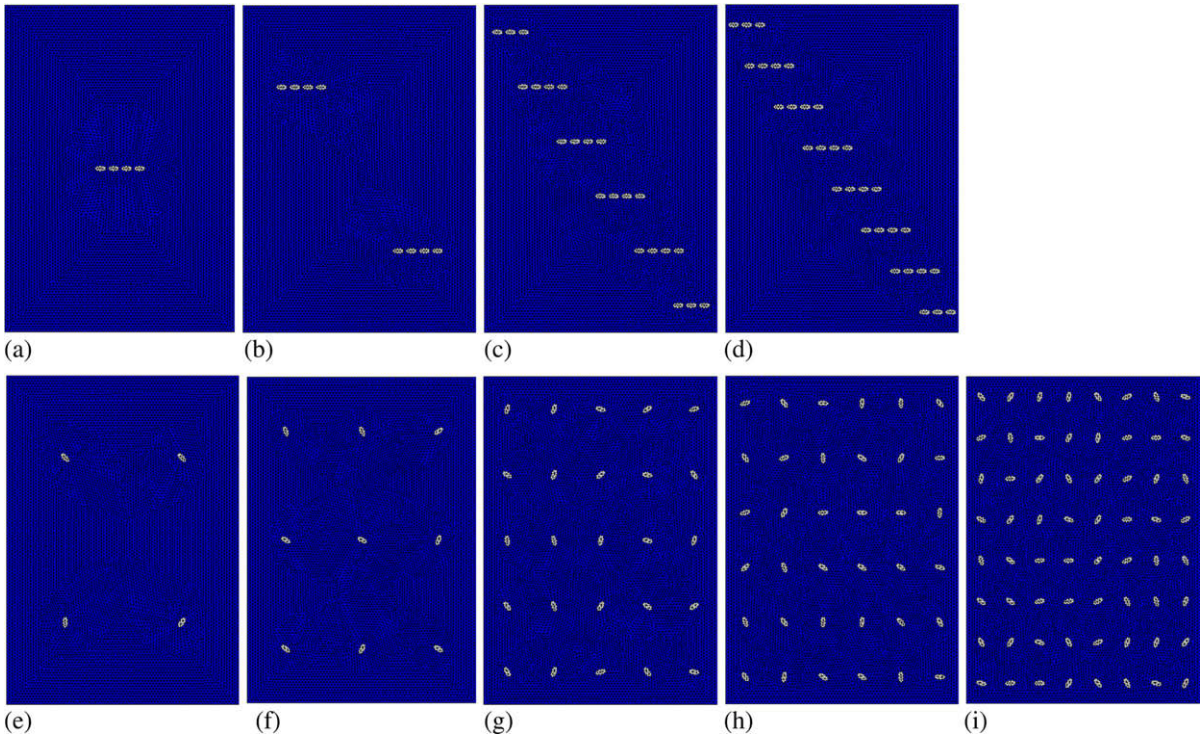

Fig. 12. The models with variation of volume fraction of particles with (a)–(d) stringer distribution and (e)–(i) uniform distribution.

trix material is rather ductile, is not controlled by a single large particle or by the most damaging stringer, although they may become preferential places of damage initiations. More particles or stringers can provide multiple damage sources which can make the damage propagate faster and cause early failure and fracture. On the other hand, the fracture strains are much smaller in the models with stringer distribution than with uniform distribution. This indicates that not only the particle volume fraction, but the particle distribution plays a very important role in controlling the post-necking and damage processes.

More detailed studies are performed on particle distribution by models containing 16 particles where distributions varied from random/uniform to stringer distribution. For the stringer distribution, the stringer length, i.e. the number of particles in each stringer, is varied. It is interesting to find that the results of random distribution are similar to that of uniform distribution. It must be noted here that the random distribution is not completely random. It is not possible to generate a statistically good random distribution of particles with such a small particle field containing only 16 particles. The models of random and uniform distributions show larger post-necking deformation and fracture strains, and the topography of the fracture surface indicates that the models are more prone to cup–cone type failure. The models of stringer distributions, on the other hand, show quite different results where shear-type failures are observed and smaller post-necking deformation and through-thickness thinning are experienced before final fracture. These modeling observations are again consistent with experimental observations of different behaviors during uniaxial tension of AA5754 CC and DC alloys with similar Fe contents of 0.21 wt.%, where the former (CC) has stringer dominant particle distribution, while the later has more random particle distribution (Kang et al., 2007). For the models of stringer distributions with different stringer length (n_s), it is quite interesting that the fracture strains decrease with stringer length firstly, but shortly after the fracture strains increase. These results are explained by the fact that longer stringer length (n_s), fewer stringers or damaging sources exist in the model. As described previously, more damaging sources will help the damage propagation and cause earlier failure. This explains the increase of fracture strains with stringer length. On the other hand, the damage source can easily move away from the damage path during deformation when the stringer is very short. The reason for this practice of putting all stringers along the diagonal of the model in this current work is because it is very difficult to generate real random distribution of stringers in such a small particle field, which therefore would not give consistent results between models. It must be admitted that this special distribution of stringers is a simple and extreme case, but gives comparable results between models. A real random distribution is only possible for a large particle field (Hu et al., submitted for publication). The larger fracture strain and cup–cup type topography of the model of a single long stringer of 16 particles in the center of the model imply that the post-necking and facture limits can be enhanced in a material if the second phase hard particles are segregated into the center plane through the thickness. This can be even more beneficial for bendability.

Although very small particle fields are used in the current work, the conclusions for various parameters such as the influence of particle volume fractions and particle distributions on post-necking deformation and damage topology are consistent with that of a large particle field (Hu et al., submitted for publication). As for the influence of stringer length on post-necking behavior of randomly distributed stringers, an analytical model was proposed to calculate the number of initial damage sources which correlates with results of models (Hu et al., submitted for publication). It is impossible for the large particle model to use a well refined mesh which could realistically represent the particle shape due to computation limitation.

Finally, it needs to be addressed that the use of the edge-constrained plane strain model is a very simple method for studying the post-necking behavior and fracture in uniaxial tension. The real problem is three dimensional; it is always desirable to use three-dimensional models for a precise prediction, but is very computation demanding. Like the plane stress pre-necking model where the variation of through-thickness strain is overestimated (Hu et al., 2008c), the plane strain post-necking model would overestimate the stress and planar strain variation of the modeling plane. The current method, however, does capture the major trends and influences of different parameters of particle distribution on post-necking deformation, fracture limit and topolography of fracture surface after the material deformation is localized and the results are all consistent with experimental observation.

As stated in our previous work on the two particle plane stress models (Hu et al., 2007), the mesh sensitivity is an important numerical issue in the finite element study of strain localization. The finer the mesh, the smaller the localization strains are expected. But the trends of evolution of these strains with alignment and interparticle spacing are always consistent; only the values of strains are smaller. In the current qualitative studies which do not aim to provide a precise, quantitative prediction of behavior, we have kept the same meshing parameters for all the models.

7. Conclusions

Particle shape, volume and distributions are important factors that influence post-necking deformation. Models with elliptical particles show less post-necking than models with circular particles. When the particles are distributed as stringers, much less post-necking ductility and fracture mode is shown than in the cases where the particles are distributed randomly or homogeneously. The results show that particles with high aspect ratio (i.e. long particles), higher volume fraction of particles and stringer distribution of particles are detrimental to post-necking deformation, i.e. material bendability. In addition, stringer particle distribution can cause a shear type failure mode. The particles clustering in the center plane of material through the thickness can be beneficial for material post-necking deformation and bendability of AA5754 aluminum sheets.

Acknowledgements

This work was performed under the funding of General Motors of Canada and the Natural Science and Engineering Research Council of Canada (NSERC).

References

ABAQUS Inc., 2006. ABAQUS Manual Version 6-5.1.
Carsley, J., Kim, S., 2007. Warm hemming of magnesium sheet. Journal of Materials Engineering and Performance 16, 331–338.
Datsko, J., Yang, C.T., 1960. Correlation of bendability of materials with their tensile properties. Journal of Engineering for Industry 82, 309–314.
Hu, X.H., Van Houtte, P., Liebeherr, M., Walentek, A., Seefeldt, M., Vandekinderen, H., 2006. Modeling work hardening of pearlitic steels by phenomenological and Taylor-type micromechanical models. Acta Materialia 54, 1029–1040.
Hu, X.H., Wilkinson, D.S., Jain, M., Mishra, R.K., 2007. Modeling the influence of grain-level matrix inhomogeneity on strain localization in the presence of hard particles. Modelling and Simulation in Materials Science and Engineering 15, 893–909.
Hu, X.H., Jain, M., Wilkinson, D.S., Mishra, R.K., 2008a. Microstructure-based finite element analysis of strain localization behavior in AA5754 aluminum sheet. Acta Materialia 56, 3187–3201.
Hu, X.H., Wilkinson, D.S., Jain, M., Mishra, R.K., submitted for publication. A parametric study of the effect of particle distribution on post-necking deformation and fracture topography in AA5754 aluminum alloy sheets by an edge-constraint plane strain model. International Journal of Plasticity.

Hu, X.H., Wilkinson, D.S., Jain, M., Mishra, R.K., 2008c. Modeling strain localization using a plane stress two-particle model and the influence of grain level matrix inhomogeneity. Journal of Engineering Materials and Technology 130, 021002.

Kang, J.D., Wilkinson, D.S., Malakhov, D.V., Halim, H., Jain, M., Embury, J.D., Mishra, R.K., 2007. Effect of processing route on the spatial distributions of constituent particles and their role in the fracture process in AA5754 alloy sheet materials. Materials Science and Engineering A 456, 85–92.

Marciniak, Z., Duncan, J.L., Hu, S.J., 2002. Mechanics of sheet metal forming, second ed. Butterworth-Heinstein, Woburn, MA.

Sarkar, J., Kutty, T.R.G., Conlon, K.T., Wilkinson, D.S., Embury, J.D., Lloyd, D.J., 2001. Tensile and bending properties of AA5754 aluminum alloys. Materials Science and Engineering A 316, 52–59.

Sarkar, J., Kutty, T.R.G., Wilkinson, D.S., Embury, J.D., Lloyd, D.J., 2004. Tensile properties and bendability of T4 treated AA6111 aluminum alloys. Materials Science and Engineering A 369, 258–266.